Energy Conversion and Management: X 8 (2020) 100056

Contents lists available at ScienceDirect

Energy Conversion and Management: X

journal homepage: www.journals.elsevier.com/energy-conversion-and-management-x

Development of a hardware-in-the-loop simulator for small-scale concentrated solar combined heat and power system

Luca Cioccolanti[a,*], Roberto Tascioni[a,b], Matteo Pirro[c], Alessia Arteconi[d,e]

[a] CREAT, Università eCampus, Via Isimbardi 10, 22060 Novedrate, CO, Italy
[b] DIAEE, Sapienza Università di Roma, via Eudossiana 18, 00184 Roma, Italy
[c] Società di Trasferimento Tecnologico e Guida all'Innovation Engineering, S.TRA.TE.G.I.E. srl, Via Sandro Totti 3, 60131 Ancona, Italy
[d] KU Leuven, Department of Mechanical Engineering, B-3000 Leuven, Belgium
[e] DIISM, Università Politecnica delle Marche, Via Brecce Bianche 1, 60131 Ancona, Italy

ARTICLE INFO

Keywords:
Renewable energy
Concentrated solar thermal power
mCHP
HiL simulator
Operation control
Control strategy optimization

ABSTRACT

In this work a hardware-in-the-loop (HiL) simulator of a novel micro combined heat and power system is presented and its use for control algorithm optimization is demonstrated and discussed. The plant under investigation consists of a concentrated Linear Fresnel Reflectors solar field, a 2 kWe/18 kWt Organic Rankine Cycle unit and an advanced latent heat thermal energy storage tank equipped with reversible heat pipes as developed by a consortium of universities and companies within the EU funded project Innova Microsolar. A smart control unit manages their integration and monitors the operation of each subsystem.

In order to support the optimization of the control algorithms and the definition of the best control strategy of the micro-CHP plant at different working conditions, a simulation framework based on Matlab/Simulink has been developed by the authors and connected to the real control unit according to a HiL approach. Ad-hoc models of the different subsystems together with those of the components (i.e. valves and variable speed pumps) regulating the plant operation have been included.

The use of the HiL simulator has permitted to optimize the control logic of the integrated plant prior to its future commissioning, thus helping to overcome some of the technical and reliability issues occurring during the setup of the real system. In particular, the HiL has allowed: (i) to define the proportional and integral gains of the diverters in order to assure a robust and fast response of the plant during the switch among the different operation modes; (ii) to prove the limits of acting on the oil pump flow rate in assuring the nominal oil temperature at the inlet of the ORC unit, due to the inherent fluctuations caused by this control strategy; and (iii) to assess the best control strategy which is obtained by acting on the aperture of the diverter which controls the oil mass flow rate to the ORC unit. Hence, the scientific approach here proposed can be extended also to many other complex energy conversion systems in order to significantly reduce the potential critical issues during their commissioning.

1. Introduction

Among the key instruments to reach the challenging targets established in the Paris Agreement, energy transition based on renewable technologies plays a fundamental role [1]. Because of its worldwide availability, solar energy represents the most promising and clean energy for future power generation. In particular, the use of solar energy in decentralized energy systems is foreseen as a valuable alternative to substitute thermal and electric power generation from fossil fuel. As a matter of fact, off-grid solar energy has been one of the fastest growing industries in providing energy access in recent years [1]. Despite that, the structural expansion of decentralized micro-Combined Heat and Power (mCHP) systems has been limited so far because of technological issues and lack of regulatory schemes [2]. Moreover, when coupled with unpredictable renewable energy sources, such as solar, the short and long-term fluctuations of these systems entail challenging dynamic effects to deal with. To reduce such variability and extend the operation of the systems, energy storage technologies can be usefully adopted. Over the years many researchers have focused on the development of different storage technologies and in particular Thermal Energy Storage (TES) technologies for Concentrated Solar Power (CSP) [3]. For example, Cabeza et al. [4] investigated a new concept of thermochemical

* Corresponding author.
E-mail address: luca.cioccolanti@uniecampus.it (L. Cioccolanti).

https://doi.org/10.1016/j.ecmx.2020.100056
Received 13 June 2020; Received in revised form 19 August 2020; Accepted 22 August 2020
Available online 27 August 2020

Nomenclature

A	cross sectional area of the valve [m^2]
A_{sf}	area of the primary collectors [m^2]
c_1	first order heat losses coefficient [kW/(m·°C)]
c_4	fourth order heat losses coefficient [kW/(m·°C^4)]
c_p	specific heat at constant pressure [J/kg·°C]
CHP	Combined Heat and Power
CSP	Concentrated Solar Power
DNI	Direct Normal Irradiation [kW/m^2]
D_{int}	internal diameter of the tube [m]
IAM	Incident Angle Modifier
HiL	Hardware-in-the-loop
L_{abs}	length of the absorber tubes [m]
LHTES	Latent Heat Thermal Energy Storage
LFR	Linear Fresnel Reflector
OM	Operation Mode
ORC	Organic Rankine Cycle
E_{gen}	electric energy generated [kWh_e]
F	friction factor
K	additional pressure losses coefficient
K_v	flow rate that generates a pressure drop of 1 bar in the valve [m^3/h]
$K_{v,corr}$	corrected K_v value of the valve [m^3/h]
K_{vs}	flow rate that generates a pressure drop of 1 bar when the valve is opened at its maximum [m^3/h]
$\dot{m}$	mass flow rate [kg/s]
$\dot{m}_c$	mass flow rate of the cooling water [kg/s]
$\dot{m}_{control}$	ratio of the mass flow rates in the valve
$\dot{m}_f$	mass flow rate of the working fluid in the ORC unit[kg/s]
$\dot{m}_{LFR}$	mass flow rate of the oil in the solar field [kg/s]
$\dot{m}_{ORC}$	mass flow rate of the oil permitted by the ORC unit [kg/s]
$\dot{m}_{pump}$	mass flow rate of the oil in the main pump [kg/s]
n_{90}	number of bends
P	wetted perimeter of the cross sectional area [m]
PCM	Phase Change Material
P_{LFR}	power to/from the LFR [kW]
P_{TES}	thermal power to/from the TES [kW_t]
P_{ORC}	thermal power to/from the ORC [kW_t]
$P_{ORC,el}$	electric power produced by the ORC [kW_e]
PI	Proportional Integral
PID	Proportional Integral-Derivative
Q	volumetric flow rate [m^3/s]
Q_{loss}	heat losses at the receiver [kW_t]
Q_{TES}	thermal energy to/from the TES [kJ]
$Q_{TES,loss}$	heat losses of the TES [kW_t]
$Q_{tube,loss}$	heat losses of the tubes [kW_t]
R	rangeability of the valve
$R_{conv,ext}$	external convective resistance [(°C·m)/W]
Rcond	conductive resistance [(°C·m)/W]
Re_{seat}	Reynolds number in the valve seat
TES	Thermal Energy Storage
T_{abs}	average temperature of the absorber tube [°C]
T_{LFR}	temperature of the oil from the LFR solar field [°C]
$T_{ORC,off}$	lower bound temperature set-point of the TES [°C]
$T_{ORC,on}$	upper bound temperature set-point of the TES [°C]
$T_{TES,av}$	average temperature of the TES [°C]
$T_{TES,in}$	inlet temperature of the oil to theTES [°C]
$T_{TES,out}$	outlet temperature of the oil from the TES [°C]
T_{in}	inlet temperature of the cooling water at the condenser [°C]
T_{out}	outlet temperature of the cooling water at the condenser [°C]
U	oil velocity along the x direction [m/s]
V_{ap}	aperture of the valve
V	velocity [m/s]

Superscripts and subscripts

1	straight outlet of the valve
2	bended outlet of the valve
I	i-th cross section along x direction
In	inlet
J	j-th along the radial direction
K	k-th time step
Min	minimum
Max	maximum
Out	outlet
Oil	oil
Set	set point

Greek symbols

A	solar elevation angle
E	roughness of the surface
Δh_e	actual specific enthalpy difference across the expander [kJ/(kg K)]
Δh_p	actual specific enthalpy difference across the pump [kJ/(kg K)]
Δp_t	pressure losses in the tube [Pa]
Δp_v	pressure losses in the valve [Pa]
ΔT_{TES}	temperature difference between the PCM and the oil [°C]
$\Delta t_{int\text{-}timestep}$	time interval of the internal time step [s]
Δx	finite space difference along the longitudinal direction x [m]
Δt	finite time difference [s]
η_{el}	electrical efficiency
η_m	mechanical efficiency
η_{opt}	optical efficiency
$\eta_{opt,max}$	maximum optical efficiency
η_{rec}	receiver efficiency factor
ρ_{oil}	oil density [kg/m^3]
ν_{oil}	oil kinematic viscosity [m^2/s]
Σ	solar azimuthal angle
Θ	solar incident angle
$\tau_{TES,latent}$	time constant of the TES during the melting phase [min]
$\tau_{TES,sensible}$	time constant of the TES during the sensible phase [min]

storage based on consecutive reactions to be coupled with a CSP plant with solar central receiver. Bravo et al. [5], instead, performed a multi-objective optimization to find the best operational strategy of a hybrid PV-CSP plant with a thermochemical storage system based on calcium-looping process finding that such a TES allows enhancing dispatch-ability and plant competitiveness. Nevertheless, in CSP applications sensible or latent heat technologies are usually adopted so far. With respect to the latter, Costa et al. [6] designed a latent heat thermal storage system (LHTES) using solar salt as phase change material to be coupled with a small-scale concentrated solar plant based on Linear Fresnel Reflectors (LFR). In another paper, Liu et al. [7] investigated different energy storage media for a shell-and-tube TES for CSP plants. In their work, the authors found that PCM-graphite-PCM sandwich configuration increased the energy density of about 28.7% compared to the single graphite configuration. Among the different integrated systems to efficiently convert solar energy into generated power, CSP plants coupled with Organic Rankine Cycle (ORC) systems are considered one of the most competitive at large scale [8]. At small-scale,

instead, their adoption is still limited so far mainly because of economic feasibility [9]. Hence, many efforts have been made by academia and industry to achieve advancements and make them cost-competitive. For example, Bouvier et al. [10] studied and tested the performance of a single-cylinder expander coupled with a 46.5 m^2 double-axis PTC solar field, obtaining a power output of 1.3 kWe and a solar-to-electricity efficiency of 3%. Freeman et al. [11] numerically investigated the performance of solar CHP ORC by comparing the electrical power output from concentrating parabolic trough collectors and non-concentrating evacuated tube collectors. According to their work, authors demonstrated that for the UK climate the average power output of the ORC is almost the same with both type of collectors. Rady et al. [12] conceptually designed and thermodynamically analysed a small-scale multi-generation concentrated solar ORC plant for a medical center building in Egypt. They compared the output of the system using both parabolic trough collectors and linear Fresnel reflectors, finding that a careful design and operation of the plant is needed to increase the overall plant efficiency and economic value. Villarini et al. [13], instead, numerically investigated and compared the performances of two innovative small-scale ORC trigeneration plants based on compound parabolic collectors and LFR with varying incident radiation. Authors found that whenever cooling demand is predominant, LFR has to be preferred. Eventually, Ni et al. [14] assessed the dynamic performances of a small-scale ORC plant driven by parabolic through collectors under clear sky and cloudy sky conditions. Based on the response of the systems to the sky conditions, the authors found that the optimized system implementing a conventional Proportional Integral-Derivative (PID) control strategy can generate almost 20% more energy than the system without control in a time span of 25,000 s during a cloudy sky day.

Independently from the solar ORC configuration, an adequate control logic and management of the integrated systems are of paramount importance to better exploit the collected solar energy and increase the conversion efficiency of such plants. However, generally speaking, the development and test of physical prototypes can be very expensive. Hence, use of powerful development tools is crucial to properly set up complex energy systems while minimizing the probability of errors, reducing the design time and the related costs. In order to minimize such costs, two approaches are commonly adopted: (i) simulation and (ii) hardware-in the-loop (HiL). In general the former allows to provide an estimation of the performance and of the main critical working conditions. However, when the dynamics of the systems need to be accurately taken into account, more powerful tools are required such those based on HiL approach. This approach, indeed, shows several interesting advantages, such as easy validation of control logic, discarding ineffective logics and optimizing the more promising ones. Therefore, once implemented in a simulator, the HiL technique allows reducing the required time for the development of the control algorithms of a real control system, since physical phenomena can be simulated and developers can concentrate most of their efforts directly on the control algorithms performances and optimization [15].

In literature, many researchers have addressed the use of the HiL technique to evaluate various optimizations of energy conversion systems operation. For example, Mohammadi et al. [16] developed an electromechanical emulator to study the behaviour of wind turbines during faults thus providing a useful tool to design more economical and higher performing wind turbines. Mehrfeld et al. [17] made use of the HiL concept to develop a new methodology to assess the annual performance of three energy conversion systems to be applied into buildings. In particular, a ground-source heat pump, an air-source heat pump and a Stirling engine mCHP system have been considered by the authors in their work finding good agreement between the simulated and the experimental tests results in terms of annual efficiencies. Huang et al. [18] developed an agent-based framework for HiL simulations to investigate the controller performance in buildings and the dynamics of major equipment. The potentiality of the developed HiL framework was then shown by controlling the speed of the supply fan in the air handling unit of a variable-air-volume building heating, ventilation and air-conditioning system, finding that a certain control sequence saved more than 50% of the baseline fan energy consumption. Griese et al. [19] performed HiL simulations of an integrated energy system consisting of a biocatalytic methanation reactor, a photovoltaic park, a regenerative fuel cell and short-term storage units supporting the selection of the parts or process parameters prior to any potential realization of such a system at large scale. Mayyas et al. [20], instead, integrated the HiL and the model based design approach to evaluate the energy efficiency of hybridized powertrains and tune advanced energy management strategies for their operation. Eventually, Pugi et al. [21] applied the HiL approach to optimize the turbine bypass controllers and

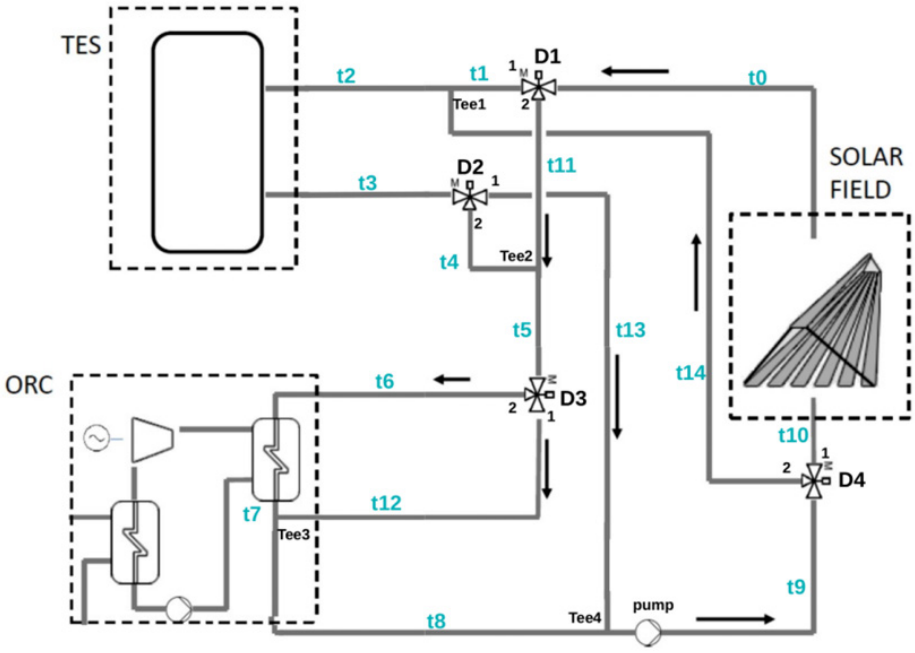

Fig. 1. Scheme of the Innova Microsolar prototype plant.

actuators used to regulate steam power plants during their transient operation.

However, to the best of the authors' knowledge none of the works available in literature applies the HiL approach to energy conversion systems based on concentrated solar technologies. In a previous work [22], the authors have evaluated the annual performance of a novel micro concentrated solar ORC CHP system design for residential applications, finding that proper control of the system was fundamental to optimize the operation of the different sub-systems with varying ambient conditions and user needs. Therefore in this work, the authors have developed a smart HiL simulator of such a plant. The main novelty of the work relies on the use of the HiL approach for small-scale CSP-ORC plants able to perform the control algorithms and plant management optimization before its real operation in the field.

2. Method and models

In this Section the methodology adopted in this work and the main characteristics of the models developed by the authors and implemented in the HiL simulator are discussed.

2.1. The integrated plant

The plant under investigation has been designed by the consortium of several EU Universities and industrial organizations under the Innova Microsolar Project [23] funded by Horizon 2020. The plant mainly consists of: (i) a 146 m^2 solar field based on Linear Fresnel Reflectors producing heat at temperatures in the range 250–280 °C; (ii) a 2 kWe/18 kWt regenerative Organic Rankine Cycle unit; and (iii) a 3.8 tons advanced PCM thermal storage tank equipped with reversible heat pipes. It has been installed in the city of Almatret (Spain) coupled to a residential building and it is going to be tested in the forthcoming months. Further details about the plant can be found in [24]. Fig. 1 shows a scheme of the plant under investigation where each tube (t), tee valve (Tee) and diverter (D) has been unequivocally identified with a progressive number to make easier the interaction of the simulator with the real control unit.

Depending on the solar radiation and the state of charge of the LHTES, the plant works according to different operation modes (OM). In OM1 the diathermic oil from the solar field, at temperature higher than 210 °C, flows directly to the ORC unit. When the collected power from the solar field exceeds the nominal power input to the ORC (about 28 kWt), the oil supplies both the TES and the ORC unit (OM4). However if the TES is already fully charged, a defocus of the LFR collector occurs (OM1def). On the contrary, when the power produced by the solar field is low or zero and the average TES temperature is within an operating range close to the melting phase ($T_{ORC,on}$ = 217 °C and $T_{ORC,off}$ = 215 °C with hysteresis), the thermal energy of the TES can be used to run the ORC unit and assure its operation for a maximum of 4 h with no sun. In particular, in OM5 only the PCM thermal energy storage supplies the ORC, whilst in OM6 both the LFR solar field and the TES supply the ORC unit. The three main subsystems above mentioned are connected each other by proportional valves which allow the operation of the system in the different OM. Indeed, the real control unit, as further detailed later on, interacts with the subsystems, the oil pump and the valves to adjust the diathermic oil mass flow rate according to Table 1.

With reference to Table 1, $\dot{m}_{ORC,min}$ and $\dot{m}_{ORC,max}$ are the minimum and maximum oil mass flow rates compatible with the ORC evaporator (equal to about 0.11 and 0.22 kg/s respectively), $\dot{m}_{LFR,max}$ the maximum oil mass flow rate in the solar field which corresponds to about 3 kg/s, P_{LFR} the collected thermal power by the LFR solar field, $P_{LFR,min}$ and $P_{LFR,max}$ the minimum and maximum collected thermal power by the LFR needed to run the ORC unit (equal to 15 kW_t and 28 kW_t respectively). Hence, in OM1 the mass flow rate of the oil varies proportionally with the Direct Normal Irradiance (DNI) up to 0.22 kg/s, while in OM4 it varies in the range 0.22–3 kg/s.

2.2. The real control unit

The designed control unit has the aim both to monitor the overall system and to control and interact with the individual components (pre-operational checks, start-up, operation monitoring, scheduling, controlled or emergency shut downs, monitoring charging and discharging of the thermal storage and on- and off-grid operation mode of the power plant). The control system has a specially developed built in software and its control algorithms have been designed to favor the use of the ORC system to cover the final user's energy demand and, in case of high DNI, to recharge as much as possible the thermal storage. In particular, the ORC thermal energy production should satisfy the domestic hot water and space heating demand, guaranteeing the highest possible energy and carbon savings.

The central control system does not have the internal control of the single subsystems, but collects information from them through a fieldbus connection. The control unit utilizes the collected information to achieve an efficient management and better integration of all subsystems. Indeed, the central control unit can manage the whole plant setup acting on the proportional valves (D1, D2, D3 and D4 of Fig. 1) and on the main pump (Table 2).

Control procedures are organized in two separate and parallel layers. The lower layer is responsible of system safety: if the system is not in a safe condition to operate, the control does not provide the enabling signal to the different subsystems, it blocks control procedures and deactivates supervision while, as soon as the system gets in a safe state, all functionalities are enabled again. The upper layer, instead, is responsible of the system control. The whole system can work in six different operating modes depending on the actual status of its subsystems and the control logic switches between these admissible phases.

The hardware architecture of the control system is reported in the following Fig. 2: an embedded PC is connected through the main switch to the external components (ORC and LFR) using Modbus TCP-IP open standard protocol. A Wago unit has been placed inside the control

Table 1
Operating conditions for the different OM of the Innova Microsolar prototype plant.

OM	Description	Pump flow rate (kg/s)
OM1def*	LFR supplies ORC	$\dot{m}_{pump} = \dot{m}_{ORC,max}$
OM1	LFR supplies ORC	$\dot{m}_{pump} = \frac{P_{LFR} - P_{LFR,min}}{P_{LFR,max} - P_{LFR,min}}(\dot{m}_{ORC,max} - \dot{m}_{ORC,min}) + \dot{m}_{ORC,min}$
OM2	System off	$\dot{m}_{pump} = 0$
OM3	LFR supplies PCM storage	$\dot{m}_{pump} = \dot{m}_{LFR,max}$
OM4	LFR supplies PCM storage and ORC	$\dot{m}_{pump} = \frac{P_{LFR} - P_{LFR,min}}{3P_{LFR,max} - P_{LFR,min}}(\dot{m}_{LFR,max} - \dot{m}_{ORC,min}) + \dot{m}_{ORC,min}$
OM5	PCM storage supplies ORC	$\dot{m}_{pump} = \dot{m}_{LFR,max}$
OM6	PCM storage and LFR supply ORC	$\dot{m}_{pump} = \dot{m}_{LFR,max}$

*Defocusing.

Table 2
Characteristic of the valves according to their datasheet [31].

Nominal diameter	50 mm
Seat diameter	40 mm
Rated travel	15 mm
K_{vs}	32
Characteristic	Linear
Hysteresis	≤1%
Actuating time for rated travel	120 s
Position feedback signal	8 bit

Fig. 2. Real control unit cabinet.

cabinet, connected to the field bus, with the aim of providing the management of digital and analog input/output.

2.3. The models of the main subsystems

The plant is modelled in Matlab/Simulink [25] and, in order to take into account the transient operation of the real plant, dynamic models of some components have been included. More precisely, the PCM storage tank and the pipelines connecting the different subsystems have been represented with dynamic models, whilst the ORC unit and LFR solar field by quasi-steady state models. Indeed, the TES and the pipelines have greater mass and, as a consequence, higher thermal inertia compared to the ORC system and to the LFR solar field (whose receiver tubes have a significantly lower extension than the plant pipelines, according to the prototype configuration). Hence, use of quasi-steady state models for the ORC system and the LFR solar field can be considered acceptable since it does not affect the relaxation time of the overall plant.

The optical efficiency of the LFR solar field varies with the position of the sun (incident angle θ) and it is calculated as in Eq. (1):

$$\eta opt = \eta opt,\ max(\theta = 0) \bullet IAM(\alpha, \sigma) \quad (1)$$

where $\eta_{opt,\ max}(\theta = 0)$ is the maximum optical efficiency achieved when the incident angle is zero and the IAM is the Incident Angle Modifier, which depends on the solar elevation angle α and the azimuthal angle σ. These values have been provided for the collector under investigation by the manufacturing company ELIANTO [26].

As regards the thermal power output from the solar field, it can be calculated as:

$$PLFR,\ out = Asf \bullet DNI \bullet \cos(\theta) \bullet \eta opt \bullet \eta rec - Qloss \quad (2)$$

where A_{sf} is the net area of the primary collectors, η_{rec} the receiver efficiency and Q_{loss} represents the heat losses at the receiver evaluated for the temperature range 100–600 °C according to Eq. (3):

$$Qloss = (c1 \bullet Tabs + c4 \bullet T4abs)Labs \quad (3)$$

The ORC unit developed and manufactured by ENOGIA [27] operates according to a regenerative cycle using NOVEC 649 as working fluid [28]. As previously mentioned also the ORC system has been modelled considering steady-state operation. The turbine isentropic efficiency varies with the operating conditions and its value is based on experimental data provided by the manufacturer. Regarding the pump isentropic efficiency, it has been assumed constant and equal to 0.7. In fact, gear pumps performance is not significantly affected by operating conditions. Heat exchangers have been modelled according to the ε-NTU method, assuming constant the overall heat transfer coefficient since the exact characterization of the plate heat exchangers was out of the scope of this work. Hence, the electric power produced by the ORC unit is calculated as in Eq. (4):

$$P_{ORC,el} = \dot{m}_f \bullet [\eta_m \bullet \eta_{el} \bullet \Delta h_e - \Delta h_p / (\eta_m \bullet \eta_{el})] \quad (4)$$

where the thermodynamic state points and the organic fluid flow rate (design value of 0.21 kg/s) are obtained at each time step according to an iterative procedure to achieve a fixed overheating temperature difference at the evaporator. Furthermore, the thermal power output is assessed as:

$$P_{ORC,out} = \dot{m}_c \bullet c_{p,c} \bullet (T_{out} - T_{in}) \quad (5)$$

where $\dot{m}_c$ is the flow rate of the cooling water, $c_{p,c}$ its specific heat and T_{in} and T_{out} the inlet and outlet temperatures of the cooling water at the condenser.

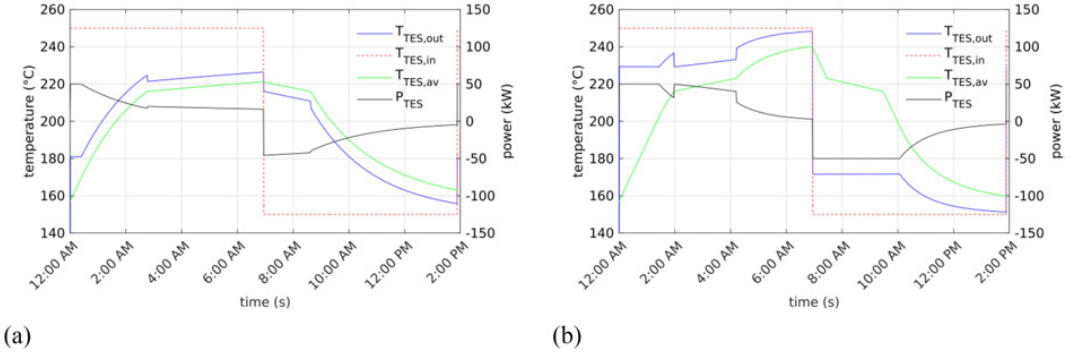

(a) (b)

Fig. 3. Dynamic behavior of the TES with oil mass flow rate: (a) at 0.3 kg/s; (b) at 1 kg/s.

The LHTES has been represented by means of a lumped model according to the guidelines of the IEA Task 32 report on advanced storage concepts [29], where a detailed description is provided. The Phase Change Material (PCM) consists of nitrate solar salt kNO_3(40 wt %)/$NaNO_3$(60 wt%), which has a high heat of fusion and a melting temperature in the range 216–223 °C. The PCM is supposed isotropic and isothermal in each internal time-step. Use of heat pipes is included in the model in terms of maximum power exchanged with the oil (40 kW) and a minimum temperature difference between the oil and the PCM (equal to 5 °C). Hence, the temperature variation of the LHTES is expressed as:

$$\Delta T_{TES(t+1)} = \Delta T_{TES(t)} \bullet e^{-[\Delta t_{int-timestep} \bullet k]} \quad (6)$$

and the heat exchanged as:

$$Q_{TES(t+1)} = \int_{t}^{t+1} P_{TES(t)} \bullet dt \quad (7)$$

The tank is 1.93 m^3 and its thermal losses calculated considering a thermal resistance of the storage of 0.4 W/m^2. In order to appreciate the dynamics of the storage unit, its performance in terms of temperature and power exchanged is assessed considering different oil flow rates as shown in Fig. 3a-b. In case of low flow rates (i.e. 0.3 kg/s as reported in Fig. 3a), the TES exhibits a time constant during the heating up $\tau_{TES,sensible}$ equal to 184 min and during the melting phase $\tau_{TES,latent}$ of about 166 min. At higher flow rates, instead, the time constants reduce significantly. For a mass flow rate of 1 kg/s the $\tau_{TES,sensible}$ and the $\tau_{TES,latent}$ correspond to 137 and 76 mins respectively.

Eventually, a one dimensional longitudinal model of the pipelines has been included, in order to take into account the influence of their thermal inertia on the plant performance. Hence, a simplified advection equation is solved for each tube:

$$\frac{\partial(\rho c_p TA)}{\partial t} + \frac{\partial(\rho u c_p TA)}{\partial x} = -Q_{loss,tube} \quad (8)$$

where ρ, c_p, T and u are the density, the specific heat, the temperature and the axial velocity of the oil respectively, A the internal cross section area of the tube, $Q_{loss,tube}$ the thermal power losses of the tube.

Eq. (8) can be rewritten by applying the one order explicit upwind scheme as follows:

$$\frac{T_{i,j}^{k+1} - T_{i,j}^{k}}{\Delta t} + u_i \frac{T_{i,j}^{k} - T_{i-1,j}^{k}}{\Delta x} = -\frac{T_{i,j}^{k} - T_{amb}}{(R_{conv_i,ext} + R_{i,cond})\rho^k c_{p_i}^k A} \quad (9)$$

where $R_{conv,ext}$ is the external convective resistance, R_{cond} the conductive resistance, k = 1,2,…,N is the number of time steps, i = 1,2,…,M the number of longitudinal segments while j = 1 ∀ k.

Also for the pipelines, their dynamics is preliminary evaluated with varying mass flow rate and temperature of the oil. For the sake of clarity, the case of OM1 is shown in Fig. 4a-b. In this operation mode, according to Fig. 1, tubes t0, t5, t6, t7, t8, t9, t10 and t11 are connected for a global length of about 37 m (based on the values reported later on in Table 3). As can be clearly noticed in Fig. 4a, for a given inlet temperature (i.e. 250 °C), the oil takes a significant amount of time prior to rise in temperature at low mass flow rate. Specifically, more than 10 min are needed to achieve a steady state temperature in case of an oil mass flow rate of 0.22 kg/s and even a higher delay occurs for 0.11 kg/s. Moreover, in this case the peak temperature reached by the oil is reduced of about 15 °C, due to the significant thermal losses of the tubes. In particular, the overall time delay to reach 63% of the peak value accounts to 1.56 mins, 7.03 mins and 13.98 min with 1 kg/s, 0.22 kg/s and 0.11 kg/s respectively. Instead, the dynamics of the tubes is not significantly influenced by the temperature of the oil as seen in Fig. 4b, thus confirming that at 1 kg/s the delays are limited.

Table 3
Characteristics of the tubes modelled in Matlab/Simulink.

Tube	Length (m)	Number of thermal nodes	n_{90}
t0	9.5	10	5
t1	0.25	2	0
t2	3	3	1
t3	3	3	2
t4	0.8	2	1
t5	2.5	3	3
t6	0.25	2	1
t7	0.25	2	0
t8	0.25	2	0
t9	2	2	1
t10	19.1	20	10
t11	3.4	4	2
t12	0.4	2	0
t13	1.5	2	1
t14	4.58	5	0

Further details on the models of the main subsystems can be found in [22,30].

2.3.1. The model of the proportional valves

In order to properly simulate the actual operation of the plant at different OM, detailed models of the valves, namely the diverters, have been also included in Matlab/Simulink. The real control unit, indeed, mainly acts on the diverters and the oil pump to control and adjust the operation of the integrated plant with varying ambient conditions and user needs.

In the Innova Microsolar prototype plant the SAMSON three-way valves 3535 (see the section in Fig. 5) have been installed, whose main characteristics utilized in the dynamic simulation are reported in Table 2:

This image appear in the datasheet of the manufacturer [31]

In general, the behavior of a valve depends on the position of the stem, its previous condition and the amplitude of the received signal. These parameters may affect the stability of the control loop because of the non-linearity phenomena induced. Therefore, the model of the valve in Matlab/Simulink (see Fig. 6) contains several blocks which

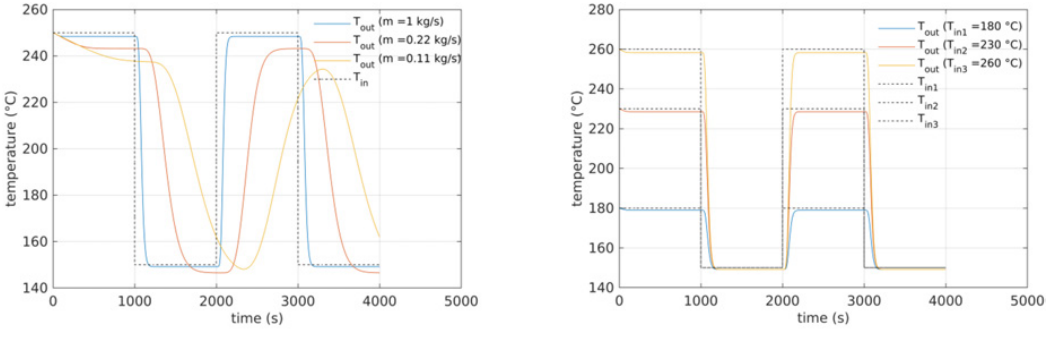

(a) (b)

Fig. 4. Dynamics of the pipelines in OM1 with varying: (a) oil mass flow rate and T_{in} = 250 °C; (b) oil temperature and$\dot{m}$ = 1 kg/s.

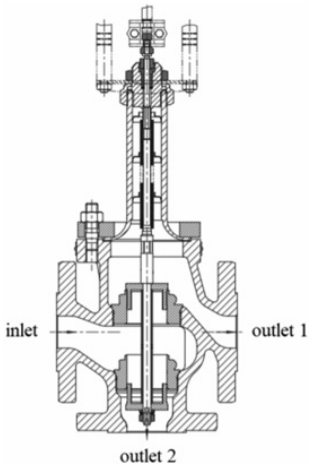

Fig. 5. Section of the diverter (three-way valve) installed in the Innova Microsolar plant.

allow representing its actual behavior. In particular: (i) the saturation block, thus including into the model the input dead-band which does not result in any output; (ii) the derivative module related to the time for displacement of the stem, thus considering the time constant of the valve needed to be in place; (iii) a resolution block (8 bit) to take into account the resolution of the valve; and (iv) the backlash block to include the hysteresis of the valve assumed equal to 1%. On the contrary, the stiction of the valve has been neglected, since it is not reported in the datasheet of the valve and it needs to be evaluated experimentally. With reference to the Innova Microsolar plant, the Electric Actuator Type 3374 [32] is installed. By using this actuator the stem of the valve takes about 120 s for the full movement of the stroke (15 mm) and the valve has a resolution of 1/256 = 0.4%.

The K_v values of the valve, which define the flow rate of the valve in each outlet generating a pressure drop of 1 bar, can be expressed as in Eqs. (10) and (11):

$$K_{v,1} = K_{vs}\left[\frac{1}{R} + \left(1 - \frac{1}{R}\right)V_{ap}\right] \tag{10}$$

$$K_{v,2} = K_{vs}\left[\frac{1}{R} + \left(1 - \frac{1}{R}\right)(1 - V_{ap})\right] \tag{11}$$

where 1 represents the straight outlet, 2 the bended outlet, K_{vs} the flow rate that generates a pressure drop of 1 bar when the valve is opened at its maximum, R the rangeability of the valve, which is defined as the ratio of maximum to minimum flow controllable through the valve, and V_{ap} is the valve aperture, which ranges from 0 to 1.

Furthermore, since the viscosity of the diathermic oil is highly affected by its temperature and in mid-temperature LFR plants the fluid is subject to significant temperature differences, a corrected $K_{v,corr}$ value is considered according to API standard 520 [33] as in Eq. (12):

$$K_{v,corr} = \frac{1}{0.9935 + \frac{2.878}{Re_{seat}^{0.5}} + \frac{342.75}{Re_{seat}^{1.5}}} \tag{12}$$

where the Reynolds number evaluated in the seat is expressed as $Re_{seat} = 4Q/P{\cdot}\nu_{oil}$, $P = 2\pi D$, with Q the volumetric flow rate, P the wetted perimeter of the cross sectional area A and ν_{oil} the kinematic viscosity of the oil.

This means that the Reynolds number depends only on the fluid dynamics of the oil through the valve. Hence, the K_{vs} values of the valve in each outlet can be assessed as:

$$K_{vs,1} = K_{v,1} \bullet K_{v,corr} \tag{13}$$

$$K_{vs,2} = K_{v,2} \bullet K_{v,corr} \tag{14}$$

whilst the corresponding pressure losses can be calculated as in Eqs. (15) and (16):

$$\Delta p_{v,1} = \frac{K_1 \rho_{oil} V_{oil}^2}{2} + 10^5\left(\frac{Q^2}{K_{vs,1}^2}\right) \tag{15}$$

$$\Delta p_{v,2} = \frac{K_2 \rho_{oil} V_{oil}^2}{2} + 10^5\left(\frac{Q^2}{K_{vs,2}^2}\right) \tag{16}$$

where K_1 e K_2 are the additional pressure losses in the straight and bended outlet respectively, ρ_{oil} the oil density and v_{oil} the oil velocity which depends on the asymmetry of the valve and its regulation.

For the sake of clarity, Fig. 7a-b report the trends of the K_{vs} values and pressure drops with the aperture in case of a linear valve, as those installed in the prototype plant in Almatret. For those calculations, an inlet mass flow rate and temperature of the oil equal to 0.2 kg/s and 10 °C have been considered.

In a real plant, the balance of the mass flow rate in each part of the circuit depends not only on the pressure drops in the valves, but also on those in each tube. Hence, in the model also the latter are taken into account according to the following Eq. (19):

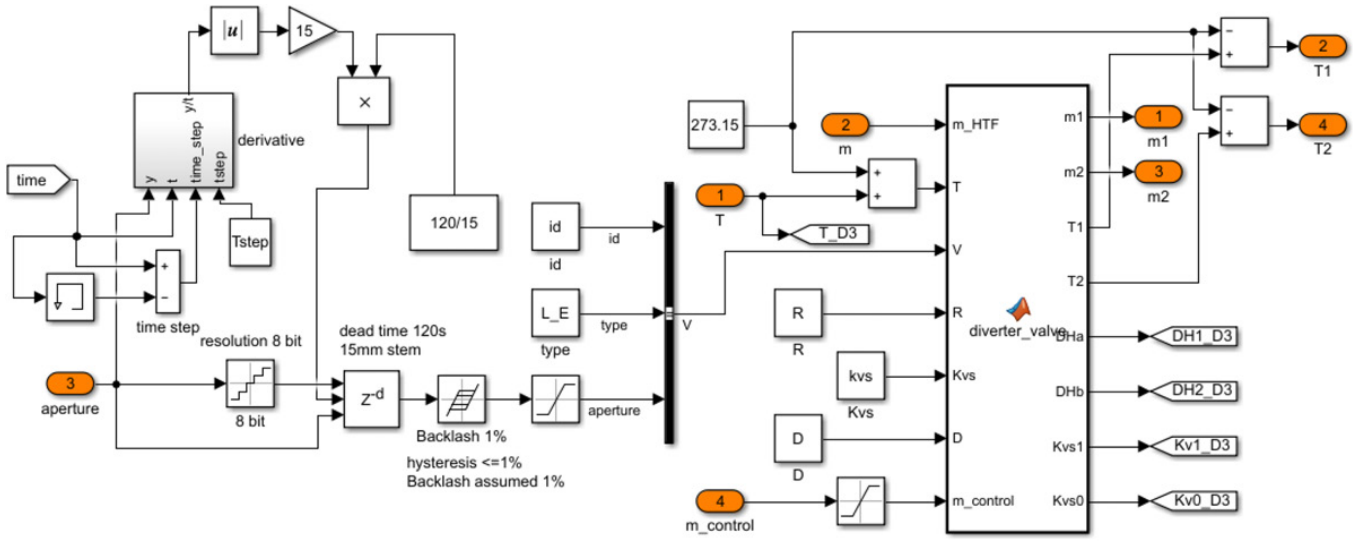

Fig. 6. The valve block in Matlab/Simulink.

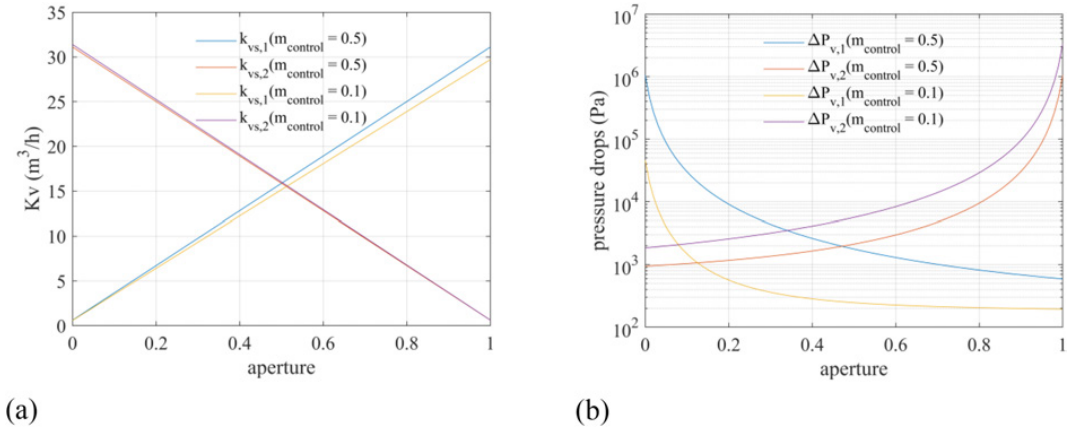

Fig. 7. K_{vs} values (a) and pressure drops (b) with the aperture for a linear valve.

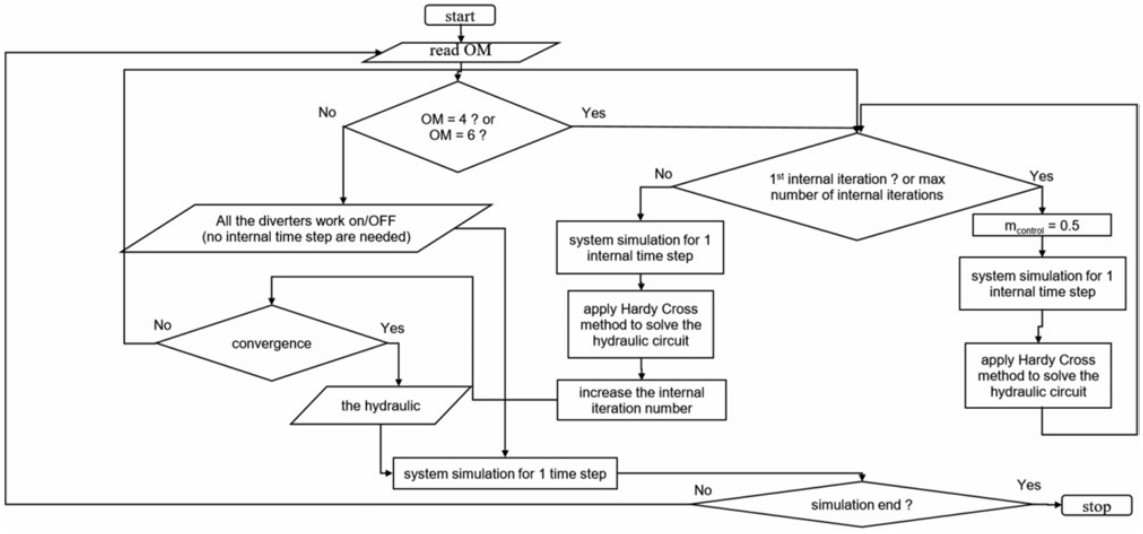

Fig. 8. The iterative procedure to solve the hydraulic circuit.

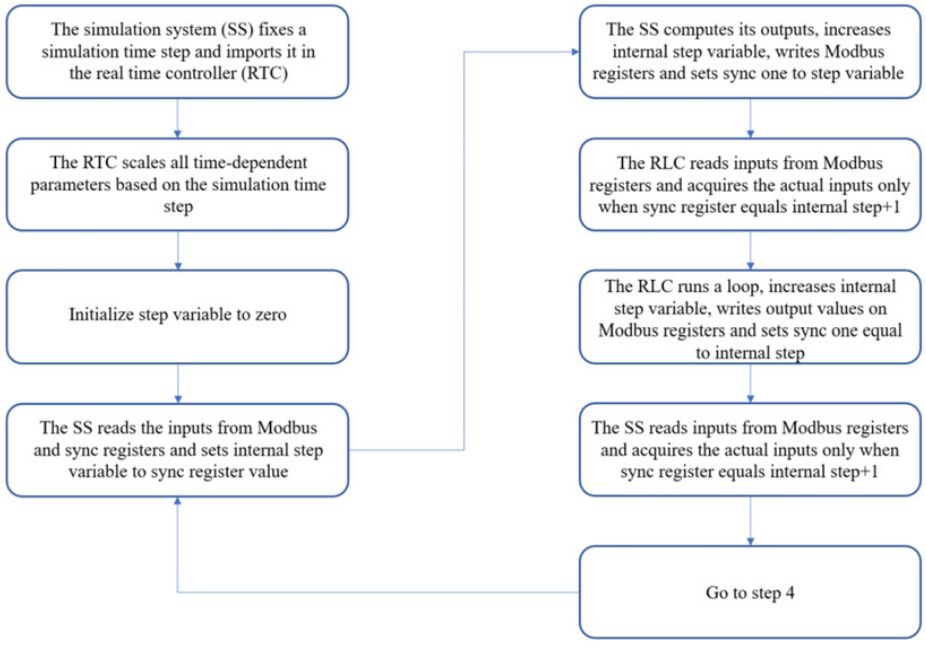

Fig. 9. The sync procedure between the simulation system and the real time controller.

Table 4
List of parameters.

Input	Parameter	Specifications
Diverters	Aperture $V_{ap,D1}$, $V_{ap,D2}$, $V_{ap,D3}$, $V_{ap,D4}$,	Discrete 1/50 range 0–1
Pump	Flow rate $\dot{m}_{pump}$	Continuous range 0–3 kg/s
Output	Parameter	Specifications
Diverters	Flow rate $\dot{m}_{D1}$, $\dot{m}_{D2}$, $\dot{m}_{D3}$, $\dot{m}_{D4}$,	Continuous range 0–3 kg/s
Linear Fresnel Reflector	Temperature $T_{LFR,out}$	Continuous 0–320 °C
	Flow rate $\dot{m}_{LFR}$	Continuous range 0–3 kg/s
Direct solar irradiance	DNI	Continuous W/m^2
Thermal Energy Storage	Temperature $T_{TES,av}$	Continuous 0–280 °C
	Flow rate $\dot{m}_{TES}$	Continuous range 0–3 kg/s
Organic Rankine Cycle	Flow rate $\dot{m}_{ORC}$	Continuous range 0–3 kg/s
Operation Mode	OM_{des}	Discrete −1–6

Table 5
Comparison between HiL simulator and Matlab/Simulink simulation model.

	Matlab/Simulink simulation	HiL simulator
$P_{LFR,in}$ [kWh]	2606.6	2606.6
$P_{LFR,out}$ [kWh]	700	699.9
$P_{TES,in}$ [kWh]	73.0	71.9
$P_{ORC,in}$ [kWh]	512.0	552.6
$P_{ORC,out}$ [kWh]	378.5	410.6
$P_{ORC,el}$ [kWh]	31.8	32.1
$Q_{TES,loss}$ [kWh]	147.3	148.1
$Q_{tubes,loss}$ [kWh]	204.0	205.7
OM1 [h]	10.57	10.57
OM2 [h]	118.10	116.06
OM3 [h]	25.25	25.25
OM4 [h]	10.81	10.81
OM5 [h]	3.27	5.31
OM6 [h]	–	–
Time of simulation [min]	27.67	273.23

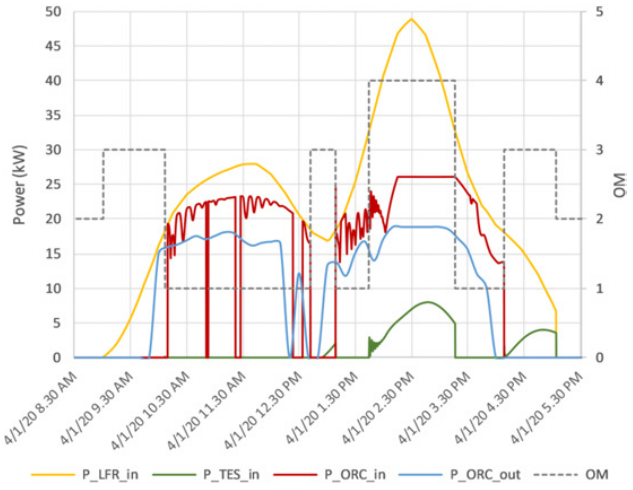

Fig. 10. Plant operation in a typical winter day.

$$\Delta p_t = f \bullet \left[\left(\frac{L}{D_{int}} \right) + n_{90} \bullet 0.3 \right] \rho_{oil} v_{oil}^2 / 2 \tag{19}$$

where D_{int} is the internal diameter of the tube, n_{90} is the number of bends at 90°, ρ_{oil} and v_{oil} are the oil density and bulk velocity respectively and f the friction factor obtained according to [34] as in Eq. (20):

$$f = \left(\frac{64}{Re} \right)^a \left[0.75 \ln \left(\frac{Re}{5.37} \right) \right]^{2(a-1)b} \left[0.88 \ln \left(\frac{6.82D}{\epsilon} \right) \right]^{2(a-1)(1-b)} \tag{20}$$

where $a = \frac{1}{1+\left(\frac{Re}{2712}\right)^{8.4}}$, $b = \frac{1}{1+\left(Re \bullet \frac{\epsilon}{150 D_{int}}\right)^{1.8}}$ and ε the roughness of the surface. In this case, the Reynolds number has been calculated based on the mean temperature and velocity of the fluid along the tube length, considering all the values of the thermal nodes. The ratio $\frac{D_{int}}{\epsilon}$ is kept constant and equal to 500, which corresponds to a very smooth surface.

Hence, according to the Innova Microsolar prototype plant installed in the city of Almatret, the following characteristics of the tubes connecting the different subsystems have been considered into the model (see Fig. 1 for the acronyms of the tubes).

Hence, the hydraulic circuit is solved by applying the 'Hardy Cross' method [35], which was originally proposed in 1936 to analyse the flow in conduits, according to an iterative procedure as summarized in Fig. 8.

This method is applicable to closed-loop pipe networks. The outflows from the system are assumed to occur at the nodes, where a node is the end of each pipe. This assumption would therefore result uniform flow in the pipelines distribution systems. Consequently, the hydraulic solution is needed only when nodes are presents, for example in OM4 and OM6, whereas in the other operating modes the oil flows in a closed loop where the stream is not divided. When all the subsystems are connected, the pressure drops are completely unknown, thus the iterative procedure starts with an initial guess value of the flow rate per each branch, by simulating the whole network (pipeline, tees, valves) the total pressure drops at the nodes can be calculated. At this point, assuming that the head loss have the simplified form $\Delta p = rQ^n$, a first order correction factor to the flow rates is applied as follow:

$$\Delta Q = \frac{-\sum rQ^2}{\sum 2rQ} \tag{21}$$

where the numerator represents the total head loss in the specific loop (by subtracting the counter-clockwise head loss from the clockwise head loss), and the denominator is the first term of the Taylor expansion. After the correction have been applied to each pipe in a loop and to all loops, a second trial calculation is made for all loops. This procedure is repeated till the flow rate variation becomes negligible. The hydraulic network is solved within an internal time step, and the external control system can only see a perfect balanced network.

The mass flow rate distribution of the diverter between the two outlets can be assumed equal to the volumetric flow rate since the fluid has the same density, thus it is calculated as:

$$\dot{m}_1 = \dot{m}_{oil} \bullet \dot{m}_{control} \tag{22}$$

$$\dot{m}_2 = \dot{m}_{oil} \bullet (1 - \dot{m}_{control}) \tag{23}$$

where $\dot{m}_{control}$ is the ratio between the mass flow rate from outlet 1 and the inlet mass flow rate to the valve.

2.4. The hardware-in-the-loop framework

Hence, the Matlab/Simulink blocks have been designed in order to interact with the real control system running on an external Programmable Logic Controller (PLC). As already mentioned in Section

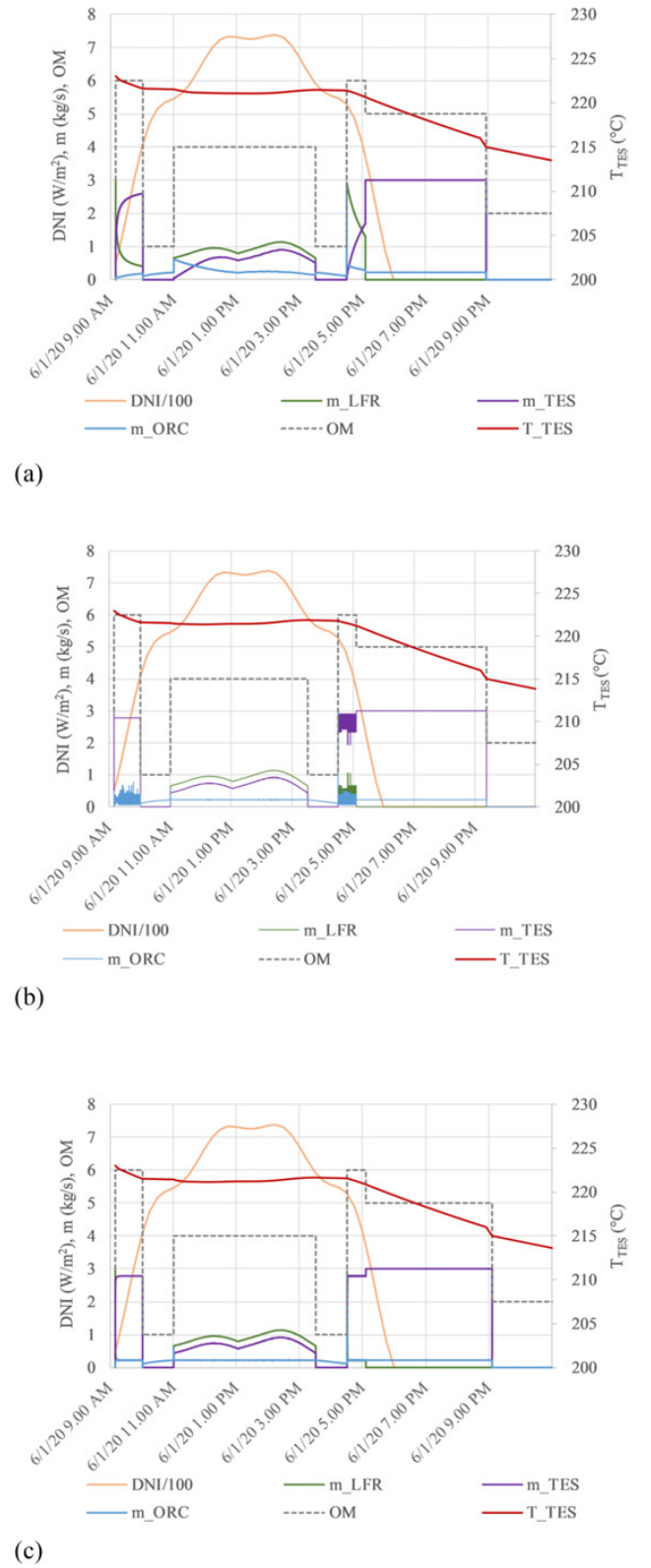

Fig. 11. Trend of the mass flow rate with varying DNI and OM for (a) small gains; (b) high gains; (c) optimal gains.

2.2, the main control unit is responsible for the monitoring of the overall system, the actuation of the system-level control procedures and the safety of the global plant. In the real system architecture this central control unit interacts in turn with the different subsystems, using a Modbus TCP-IP communication: the central controller can access all systems actuators and act as master agent. Hence, for these reasons the Matlab/Simulink blocks have been developed by the authors to emulate the subsystems control units or a part of them, following the same logic input/output as in the prototype plant.

Therefore the HiL framework consists in a simulated model of the plant running on a standard PC and in a programmable and tunable control logic running on a PLC. Potentially, once the control logic has been validated, the same software could be used in the real system as it is, because the simulated model follows exactly the real plant. However, one of the most critical aspect in a HiL system is the signal and data synchronization between components involved in the system. In particular, the simulation system (running on a standard PC) and the control system (running on a PLC) have to be synchronized. Despite the higher computational power, the former works with complex models, having configurable simulation step but no deterministic execution time. On the other hand, the second has lower computational power and processor frequency, but it is based on a deterministic cycle time.

Since the simulation time spent to complete one computational time step may differ from the hardware specification of the PC or with its actual load, a synchronization procedure is required as depicted in Fig. 9.

Therefore, according to the developed HiL approach, the Maltab/Simulink model interacts with the PLC controller with respect to the list of input and output parameters reported in Table 4:

More precisely, the diverters are regulated by means of the V_{ap} parameter (Eqs. (10) and (11)), according to their rangeability based on the datasheet of the manufacturers [31].

Another block of the valve receives as input from the PLC controller the value of its aperture, which range from 0 to 1.

3. Results and discussion

In this section the potential of the HiL simulator is presented and some significant control algorithms scenarios are presented with respect to the management of the proportional valves (D1, D2, D3 and D4 of Fig. 1) and of the main pump. Indeed, HiL technique allows to easily validate control logics, to discard ineffective approaches and to optimize the more promising ones.

3.1. The preliminary results of the HiL framework

First of all the consistency of the HiL framework is verified with respect to the Matlab/Simulink simulation in case of no interactions with the real control unit. More precisely, the performance of the plant in terms of thermal and electrical power output is assessed for a typical winter week. Weather data (i.e. solar radiation and ambient temperature) have been taken from Energy+ [36] database for the city of Lerida in Spain which is close to the town where the plant is located. Table 5 reports the cumulated thermal and electrical energy production and losses during the winter week under investigation, as well as the working hours of the system in the different OM. Moreover, the performance of the HiL approach has been compared with the simulation model also in terms of computational time. A time step of 10 s is considered and simulations run on a PC with Intel®Core G840 2.8 GHz processor.

It is evident that the obtained performance is similar between the HiL simulator and the Matlab/Simulink simulation, thus proving the conformity of the former with respect to the simulation system. In terms of computational efforts, about four hours and an half are needed to test the real control system, instead of a full week, without considering any system downtime or other mechanical or hydraulic problems that could even extend such period. At the same time, the Matlab/Simulink simulation model takes 10 times less computational time than the HiL approach. The longer amount of time of the HiL architecture respect to the simulation model is mainly due to the following two factors: firstly the communication overhead introduced by TCP-IP modbus and

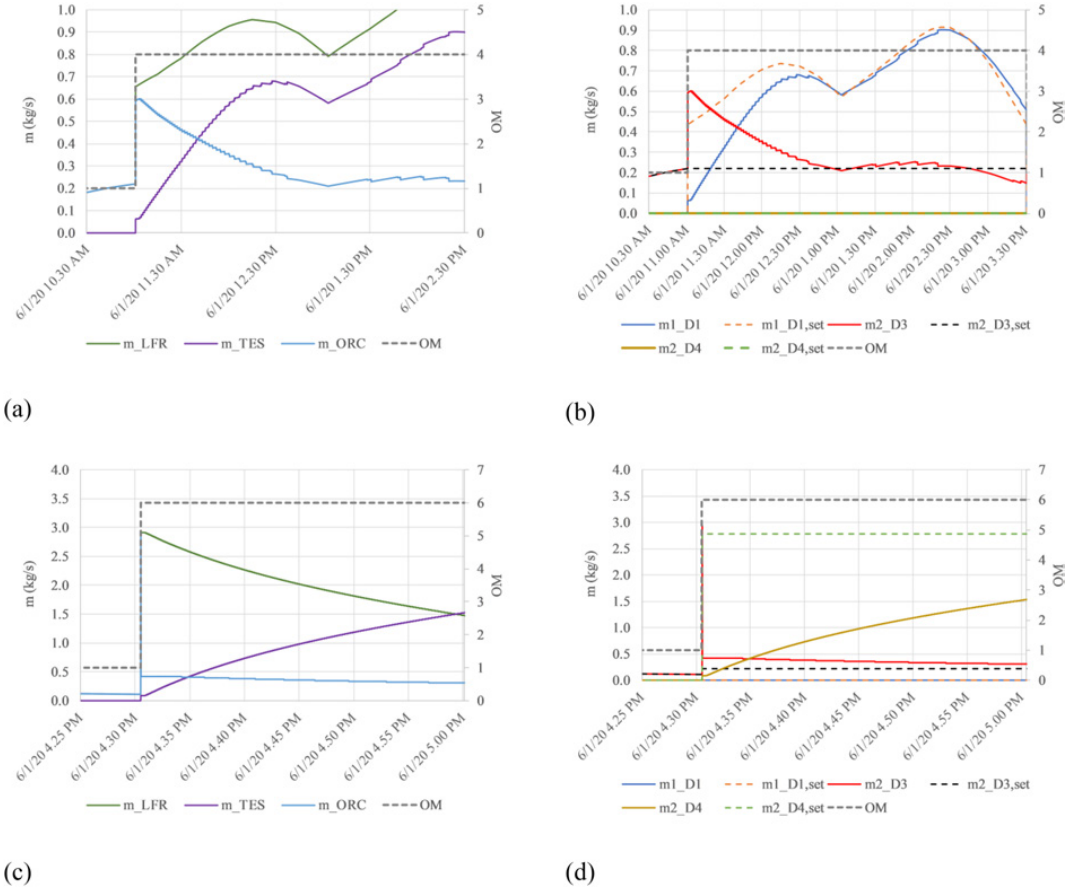

Fig. 12. Details of the mass flow rates in the different subsystems (a, c) and in the diverters (b, d) during changes of the operation mode of the plant in case of small gains.

secondly the minimum cycle time of the PLC-based control unit.

In order to better appreciate how the plant switches from an operation mode to another, Fig. 10 shows the trends of the power and the sequence of the operation mode for a typical winter day. For the day under investigation the plant works in OM1, OM3 and OM4 also. This means that even in winter time the solar field is able to supply both the ORC and TES when solar radiation is high enough. However in this case, the TES does not achieve its melting temperature and, as a consequence, does not supply the ORC when the solar radiation is low (OM5 and OM6).

3.2. Use of HiL for diverters operation

Once verified the consistency of the adopted HiL technique, the HiL simulator is firstly used to optimize the control algorithms of the plant with respect to the diverters. In particular, D1, D3 and D4 (see Fig. 1) are considered in the following analysis because of their relevance in the mass flow rate control during OM4 (LFR supplies both the LHTES and the ORC) and OM6 (both LHTES and LFR supply the ORC). A time step equal to 1 s is considered in this analysis in order to better appreciate any potential fluctuation of the flow rate. In particular, the optimal proportional and integral gains of the PI-based control are assessed during plant operation for a winter day. Hence, each PI-based controller is tuned, freezing the control output of the other controllers in order to avoid any negative interaction between the different controllers, and finally the whole system behaviour is verified with all the controllers running in parallel.

In the following, the tuning process of the controllers has been shown. HiL technique allows changing gains and parameters, appreciating immediately their effect.

Fig. 11a-c report the trend of the mass flow rates in the different subsystems of the plant with varying DNI and as a consequence OM. More precisely, trends of Fig. 11a are obtained in case of small gains of the PI-based control, those of Fig. 11b in case of high gains, while Fig. 11c shows the trends in case of the optimal gains.

Fig. 12a-b show in more detail the trend of the mass flow rates during the switch from OM1 to OM4, while Fig. 12c-d the changes from OM1 to OM6 in case of small gains. In particular, Fig. 12b and d focus on the obtained mass flow rates in the diverters under investigation with a comparison to the set-point values. As can be noticed, small gains of the integral PI-based control do not allow reaching steady state conditions in short time. Indeed, while switching from OM1 to OM4, part of the flow goes to the TES, but it takes some time prior to reach the set point (m1_D1). On the contrary, a higher amount flows to the ORC unit at the beginning. Hence, in case of such gains the plant is not able to efficiently respond to the variation of the operating conditions due to changes in ambient conditions or user needs.

On the contrary, Fig. 13a-d report the trend of the mass flow rates in the different subsystems and in the diverters in case of high gains. In this case, the system is too much sensitive to any change in the operating condition and tends to fluctuate around the set-point values in particular conditions. As can be seen in Fig. 13d, this occurs especially in OM6, when the outlet of the diverters are almost fully opened or closed and, as a consequence, a small motion of the actuator corresponds to large change in the mass flow rate. Moreover, dynamic behaviour often consists in overshooting phenomena. Therefore, also in this case the plant works in off-design conditions.

Therefore, the gains of the PI-based control have been modified until an optimum operation is achieved as reported in Fig. 14a-d. As can be clearly seen, in this case the plant achieves steady state conditions in

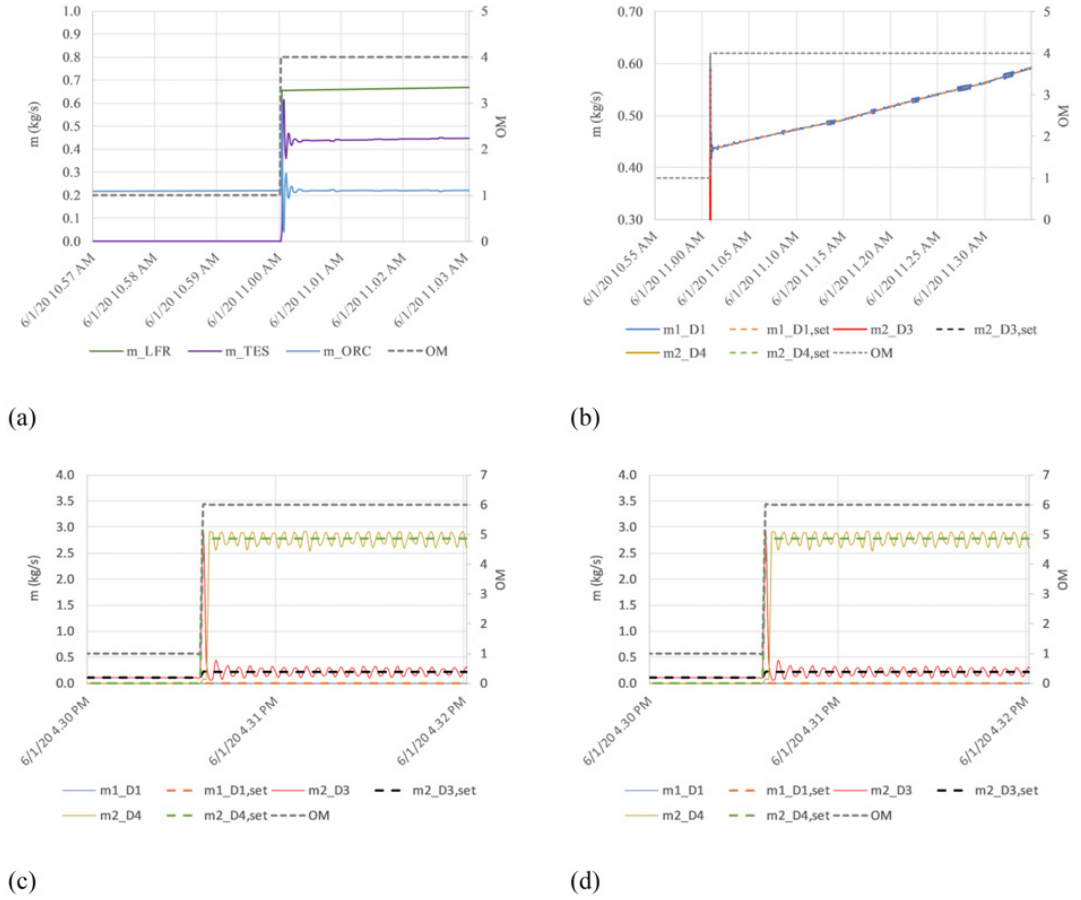

Fig. 13. Details of the mass flow rates in the different subsystems (a, c) and in the diverters (b, d) during changes of the operation mode of the plant in case of high gains.

very short time (order of magnitude of few minutes) thus proving its flexibility to varying input and constraints. During the switch from OM1 to OM4, the mass flow rate in the diverter D3 achieves the set point and, in order to comply with the small changes in the solar field, mass flow rate m2_D3 slowly fluctuates around this value due to hysteresis of the valve (< 5% of set-point value). Analogously, during the switch from OM1 to OM6 the mass flow rate in the diverter D4 reaches the set point in short time. However, in this case the fluctuations around the set point are higher, since the diverter is adjusting the flow rate near the thresholds of its operating range (operating flow rate 2.8 kg/s on a maximum of 3 kg/s).

3.3. Use of HiL for control strategy optimization

Eventually, the potential of the HiL framework is presented also with respect to the analysis of the best control strategy for the micro-CHP plant: different approaches have been tested in order to determine their pros and cons and to define the most performing one. In order to maximize the electrical power output from the ORC, the control strategy aims at assuring the nominal oil temperature of 210 °C at the inlet of the ORC unit. This set-point allows the ORC system working at its maximum electric conversion efficiency. In particular, three different control actions have been implemented: (i) acting on the oil pump to adjust the flow rate on the basis of the LFR outlet temperature; (ii) acting on the oil pump on the basis of the ORC inlet temperature; (iii) acting on the aperture of the D3 diverter on the basis of the ORC inlet temperature. For the scope of this analysis a DNI of 650 W/m^2 is considered, which causes the plant operation in OM1. In this operation mode, the mass flow rate of the oil ranges from 0.11 kg/s to 0.22 kg/s. Fig. 15a-c shows the mass flow rate of the oil and the trend of the temperatures by acting on the oil pump on the basis of the LFR outlet temperature in case of low proportional gains, low integral gains and mid gains respectively. In the first control strategy, independently from the gains, at the beginning the mass flow rate is low and, because of the high thermal inertia of the plant (pipelines etc), the oil takes a consistent time to achieve the set-point temperature of 210 °C. Indeed, more than 10 mins are required to heat up the oil loop circuit (see the initial horizontal line of $T_{LFR,out}$ in all the Figures). Once achieved the set-point, the fluctuations of the temperatures of the oil are lower in case of low integral gains, but the pump flow rate is continuously adjusted, thus extending the transient operation of the plant.

On the contrary, in case of mid gains, once the set-point temperature is achieved, the mass flow rate of the pump is reduced and achieves a steady state of about 0.14 kg/s. However, also in case of mid gains the oil achieves the nominal temperature of 210 °C at the inlet of the ORC unit with a certain delay compared to the outlet of the LFR solar field. Moreover, any change in the ORC temperature is slowly compensated, thus proving the deficiency of this control strategy in assuring the best operation of the ORC unit.

In the second control strategy, instead, the mass flow rate of the pump is adjusted based directly on the signal of the inlet temperature to the ORC. However, any adjustment of the pump flow rate is reflected in a fluctuation of the inlet temperature of the oil to the ORC unit, thus requiring a longer time prior to reach the steady state condition. In particular the distance between the sensor and the actuator can cause a delay in the action requested by the PLC, causing unwanted instability in the system. Hence, in this case a gain scheduling approach is applied once the oil achieves the set point temperature at the inlet of the ORC. More precisely, the proportional and integral gains are reduced by ten times. In this way the effect of the control action disturbs less the

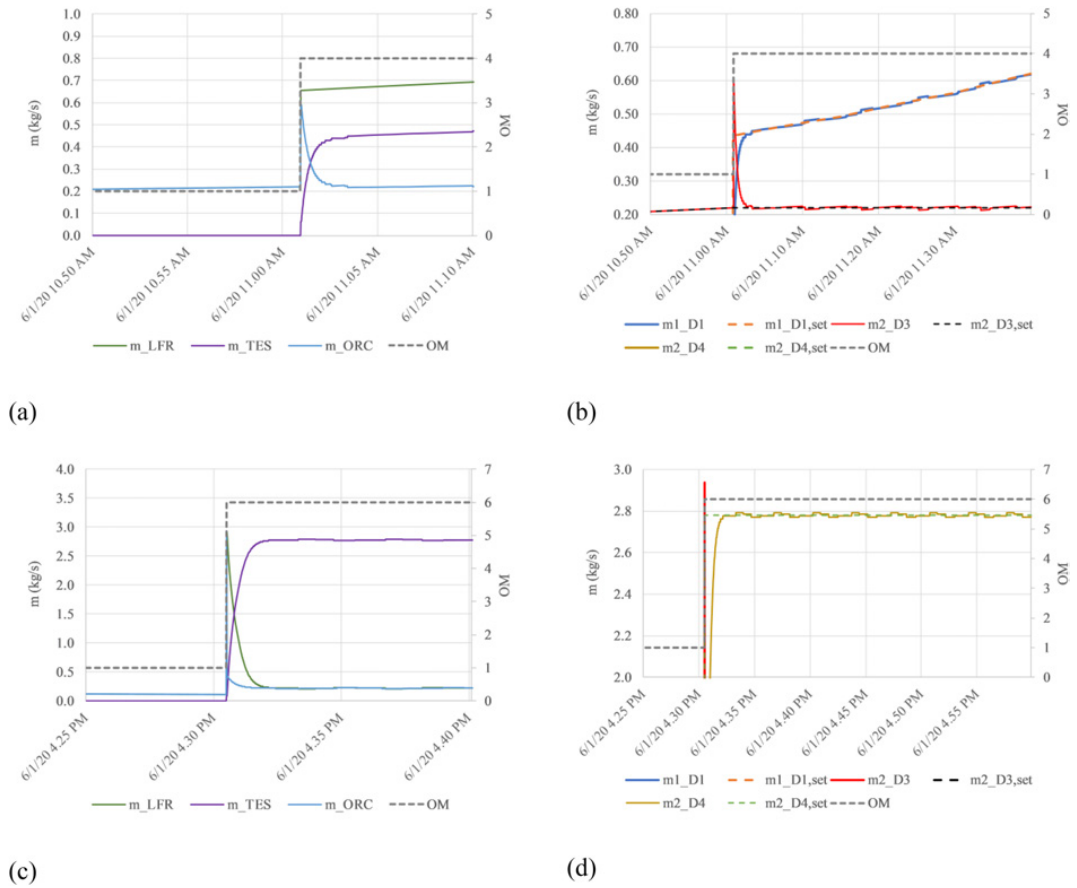

Fig. 14. Details of the mass flow rates in the different subsystems (a, c) and in the diverters (b, d) during changes of the operation mode of the plant in case of optimal gains.

stability of the system, thus reducing the fluctuations in the mass flow rate of the pump and, as a consequence, those of the oil temperature (Fig. 16).

Nevertheless, the results of both strategies highlight that an efficient and fast control of the inlet temperature of the oil to the ORC unit can not be performed by acting on the pump flow rate only. Hence, a third strategy is investigated and tuned according to which the ORC inlet temperature of the oil is controlled by acting on the aperture of the diverter D3. The effectiveness of this control strategy is evaluated for different mass flow rate of the pump, as reported in Fig. 17a-b. More precisely, in case of Fig. 17a a total mass flow rate of the oil of 1 kg/s is considered, while in case of Fig. 17b of about 0.22 kg/s. This specific value is the maximum input flow that the ORC can manage: the pump works at fixed speed, while a proportional valve can act to modulated it. From these figures it can be clearly noticed that higher overall mass flow rates entail lower fluctuations of the oil temperature at the inlet of the ORC, but at the same time longer periods for heating up the fluid. Therefore, the optimum mass flow rate of the oil pump needs to be defined as a compromise between the better operation of the ORC unit at constant operating conditions and the lower electrical power consumption of the oil pump based on the ambient conditions and the states of the different subsystems of the m-CHP plant.

4. Conclusions

In this work a hardware-in-the-loop simulator of a novel micro combined heat and power system is presented and its potential in optimizing the control algorithms and the operation of the plant is shown.

In order to properly emulate the performance of the innovative mCHP system under investigation, as designed and built by a consortium of universities and companies within the EU funded project Innova Microsolar, the HiL simulator is based on advanced mathematical models of the main components developed by the authors in Matlab/Simulink. The simulator is then coupled with the real control unit of the plant in order to support the optimization of the control algorithms prior to the experimental tests campaign.

The analysis carried out proves that such technique can be usefully and efficiently adopted to both perform the optimization of the control algorithms (PID control tuning) of the integrated system and analyse the best control strategy of the micro-CHP plant.

More precisely, the analysis has shown:

- acting on the proportional and integral gains of the diverters, it is possible to find a configuration which assures a robust and fast response of the plant during the switch from the different operation modes. It confirms the relevance of a proper tuning of the PID parameters;
- acting on the oil pump to adjust the flow rate based on the LFR outlet temperature or the ORC inlet temperature does not properly assure the best operation of the ORC unit. Indeed, with these control strategies significant fluctuations of the inlet temperature of the oil to the ORC unit occur, which cause a longer time prior to reach the steady state condition;
- the best control strategy to assure the ORC unit operation at constant operating conditions consists in circulating higher amount of oil flow rate in the solar field loop and acting on the aperture of the D3 diverter to assure the nominal ORC inlet temperature. However, the optimum mass flow rate of the oil pump needs to be defined as a compromise between the better operation of the ORC unit at constant operating conditions and the electrical power consumption of

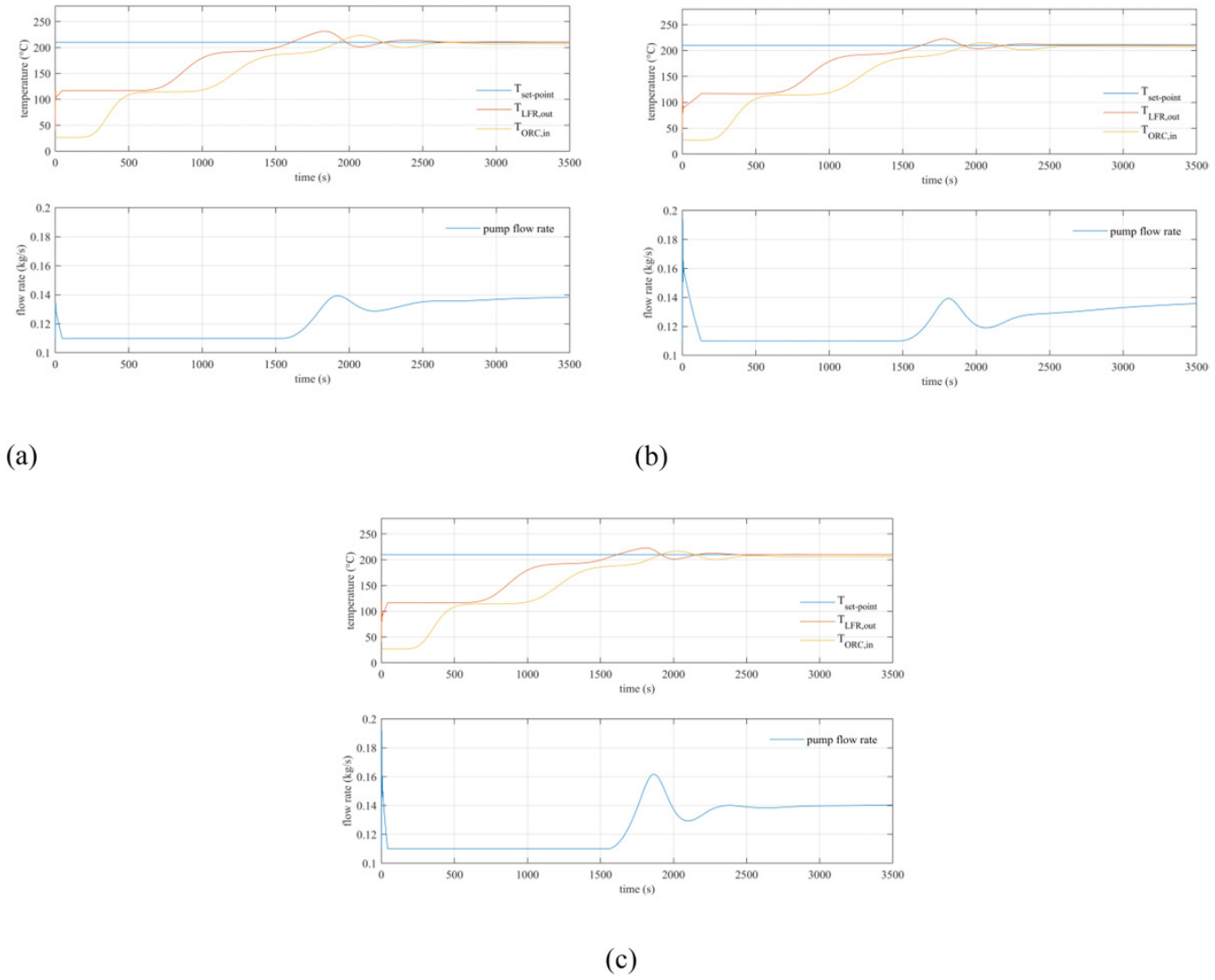

Fig. 15. a-c: Control of the mass flow rate of the pump based on the outlet temperature of the oil from the solar field; (a) low proportional gains; (b) low integral gains; (c) mid gains.

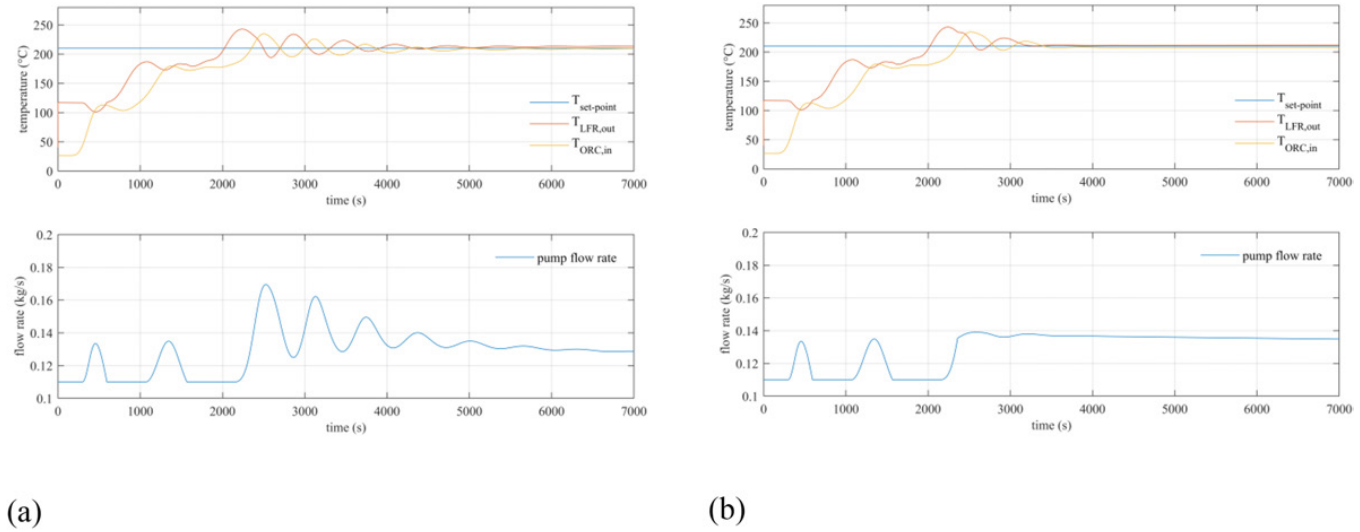

Fig. 16. a-b: Control of the mass flow rate of the pump based on the inlet temperature of the oil to the ORC unit; (a) no gain scheduling; (b) gain scheduling.

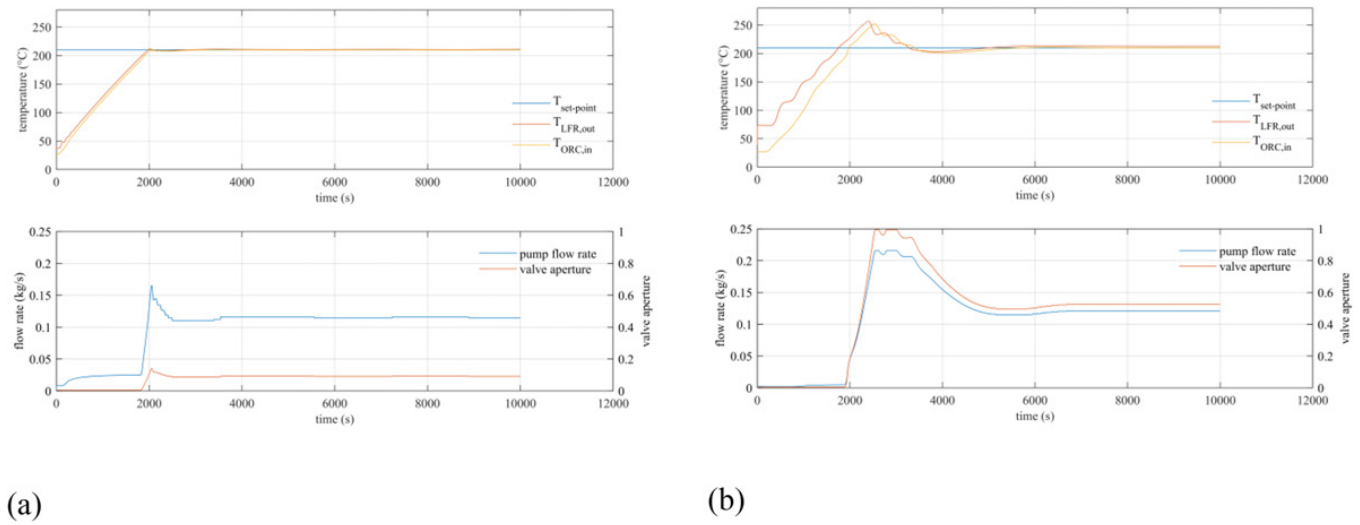

Fig. 17. Control of the inlet temperature at the ORC unit based on D3 aperture; a) total flow rate of 1 kg/s; b) total flow rate of 0.22 kg/s.

the oil pump.

Hence, the powerful effect of the developed HiL framework is demonstrated and confirmed also in case of novel configurations and integrated energy systems. In particular, the presented HiL has provided useful insights into the real operation of CSP-ORC plant with varying ambient conditions and operation modes. This aspect can significantly reduce the potential critical issues during its commissioning, supporting a smoother implementation of the real plant.

CRediT authorship contribution statement

Luca Cioccolanti: Conceptualization, Methodology, Writing - original draft, Supervision. **Roberto Tascioni:** Methodology, Software, Writing - review & editing. **Matteo Pirro:** Conceptualization, Writing - review & editing, Supervision. **Alessia Arteconi:** Writing - review & editing.

Declaration of Competing Interest

The authors declare that they have no known competing financial interests or personal relationships that could have appeared to influence the work reported in this paper.

Acknowledgement

This study is a part of the Innova Microsolar Project, funded in the framework of the European Union's Horizon 2020 Research and Innovation Programme (grant agreement No 723596).

References

[1] REN21. RENEWABLES 2017 GLOBAL STATUS REPORT. 2017.
[2] Martinez S, Michaux G, Salagnac P, Bouvier JL. Micro-combined heat and power systems (micro-CHP) based on renewable energy sources. Energy Convers Manag 2017. https://doi.org/10.1016/j.enconman.2017.10.035.
[3] Pelay U, Luo L, Fan Y, Stitou D, Rood M. Thermal energy storage systems for concentrated solar power plants. Renew Sustain Energy Rev 2017. https://doi.org/10.1016/j.rser.2017.03.139.
[4] Cabeza LF, Solé A, Fontanet X, Barreneche C, Jové A, Gallas M, et al. Thermochemical energy storage by consecutive reactions for higher efficient concentrated solar power plants (CSP): Proof of concept. Appl Energy 2017. https://doi.org/10.1016/j.apenergy.2016.10.093.
[5] Bravo R, Ortiz C, Chacartegui R, Friedrich D. Hybrid solar power plant with thermochemical energy storage: A multi-objective operational optimisation. Energy Convers Manag 2020. https://doi.org/10.1016/j.enconman.2019.112421.
[6] Costa SC, Mahkamov K, Kenisarin M, Lynn K, Halimic E, Mullen D. Solar salt latent heat thermal storage for a small solar organic rankine cycle plant. ASME 2018 12th Int Conf Energy Sustain ES 2018, Collocated with ASME 2018 Power Conf ASME 2018 Nucl Forum 2018;142:1–9. doi: 10.1115/1.4044557.
[7] Liu M, Riahi S, Jacob R, Belusko M, Bruno F. Design of sensible and latent heat thermal energy storage systems for concentrated solar power plants: Thermal performance analysis. Renew Energy 2020;151:1286–97. https://doi.org/10.1016/j.renene.2019.11.115.
[8] Aboelwafa O, Fateen SEK, Soliman A, Ismail IM. A review on solar Rankine cycles: Working fluids, applications, and cycle modifications. Renew Sustain Energy Rev 2018;82:868–85. https://doi.org/10.1016/j.rser.2017.09.097.
[9] Cioccolanti L, Tascioni R, Bocci E, Villarini M. Parametric analysis of a solar Organic Rankine Cycle trigeneration system for residential applications. Energy Convers Manag 2018;163. https://doi.org/10.1016/j.enconman.2018.02.043.
[10] Bouvier JL, Michaux G, Salagnac P, Kientz T, Rochier D. Experimental study of a micro combined heat and power system with a solar parabolic trough collector coupled to a steam Rankine cycle expander. Sol Energy 2016;134:180–92. https://doi.org/10.1016/j.solener.2016.04.028.
[11] Freeman J, Hellgardt K, Markides CN. An assessment of solar-powered organic Rankine cycle systems for combined heating and power in UK domestic applications. Appl Energy 2015;138:605–20. https://doi.org/10.1016/j.apenergy.2014.10.035.
[12] Rady M, Amin A, Ahmed M. Conceptual design of small scale multi-generation concentrated solar plant for a medical center in Egypt. Energy Procedia 2015. https://doi.org/10.1016/j.egypro.2015.12.183.
[13] Villarini M, Tascioni R, Arteconi A, Cioccolanti L. Influence of the incident radiation on the energy performance of two smallscale solar Organic Rankine Cycle trigenerative systems: A simulation analysis. Appl Energy 2019;242:1176–88. https://doi.org/10.1016/j.apenergy.2019.03.066.
[14] Ni J, Zhao L, Zhang Z, Zhang Y, Zhang J, Deng S, et al. Dynamic performance investigation of organic Rankine cycle driven by solar energy under cloudy condition. Energy 2018. https://doi.org/10.1016/j.energy.2018.01.032.
[15] Cimini G, Corradini ML, Ippoliti G, Orlando G, Pirro M. A rapid prototyping scenario for power factor control in permanent magnet synchronous motor drives: Control solutions for interleaved boost converters. Electr Power Components Syst 2014. https://doi.org/10.1080/15325008.2014.880969.
[16] Mohammadi E, Fadaeinedjad R, Moschopoulos G. An electromechanical emulation-based study on the behaviour of wind energy conversion systems during short circuit faults. Energy Convers Manag 2020;205. https://doi.org/10.1016/j.enconman.2019.112401.
[17] Mehrfeld P, Nürenberg M, Knorr M, Schinke L, Beyer M, Grimm M, et al. Dynamic evaluations of heat pump and micro combined heat and power systems using the hardware-in-the-loop approach. J Build Eng 2020. https://doi.org/10.1016/j.jobe.2019.101032.
[18] Huang S, Wang W, Brambley MR, Goyal S, Zuo W. An agent-based hardware-in-the-loop simulation framework for building controls. Energy Build 2018. https://doi.org/10.1016/j.enbuild.2018.09.038.
[19] Griese M, Hoffarth MP, Schneider J, Schulte T. Hardware-in-the-Loop simulation of an optimized energy management incorporating an experimental biocatalytic methanation reactor. Energy 2019. https://doi.org/10.1016/j.energy.2019.05.092.
[20] Mayyas AR, Kumar S, Pisu P, Rios J, Jethani P. Model-based design validation for advanced energy management strategies for electrified hybrid power trains using innovative vehicle hardware in the loop (VHIL) approach. Appl Energy 2017. https://doi.org/10.1016/j.apenergy.2017.07.028.
[21] Pugi L, Galardi E, Carcasci C, Rindi A, Lucchesi N. Preliminary design and validation of a Real Time model for hardware in the loop testing of bypass valve actuation system. Energy Convers Manag 2015. https://doi.org/10.1016/j.enconman.2014.12.061.
[22] Cioccolanti L, Tascioni R, Arteconi A. Mathematical modelling of operation modes

and performance evaluation of an innovative small-scale concentrated solar organic Rankine cycle plant. Appl Energy 2018;221:464–76. https://doi.org/10.1016/j.apenergy.2018.03.189.
[23] Innova-Microsolar n.d. http://innova-microsolar.eu/ (accessed November 3, 2017).
[24] Mahkamov K, Pili P, Manca R, Leroux A, Mintsa AC, Lynn K, et al. Development of a Small Solar Thermal Power Plant for Heat and Power Supply to Domestic and Small Business. Buildings 2018. https://doi.org/10.1115/power2018-7336.
[25] MATLAB & Simulink n.d.
[26] Elianto S.R.L - Home n.d. http://www.eliantocsp.it/index.php/en/ (accessed November 14, 2017).
[27] ENOGIA | The small turbine ORC company n.d. http://enogia.com/wp/#pll_switcher (accessed June 10, 2020).
[28] 3MTM NovecTM 649 Engineered Fluid n.d.
[29] Gantenbein P, Jaenig D, Kerskes H, Van Essen M. Final report of Subtask B " Chemical and Sorption Storage " The overview A Report of IEA Solar Heating and Cooling programme -Task 32 Advanced storage concepts for solar and low energy buildings Report B7 of Subtask B 2008.
[30] Tascioni R, Cioccolanti L, Del Zotto L, Habib E. Numerical investigation of pipelines modeling in small-scale concentrated solar combined heat and power plants. Energies 2020. https://doi.org/10.3390/en13020429.
[31] Samson AG. T 8136. 2001.
[32] Special features Type 3374 Electric Actuator. 2019.
[33] API, The American Petroleum Institute n.d. https://www.api.org/ (accessed February 27, 2020).
[34] Bellos V, Nalbantis I, Tsakiris G. Friction modeling of flood flow simulations. J Hydraul Eng 2018. https://doi.org/10.1061/(ASCE)HY.1943-7900.0001540.
[35] Cross H. Analysis of flow in networks of conduits or conductors. Eng Exp Stn 1936.
[36] EnergyPlus – Weather Data Sources n.d. https://energyplus.net/weather/sources (accessed January 11, 2019).